Progress In Electromagnetics Research M, Vol. 122, 97-105, 2023

(Received 26 October 2023, Accepted 4 December 2023, Scheduled 15 December 2023)

Dispersion Analysis of a Planar Rectangular Tape Helix Slow Wave Structures Supported by Dielectric Rods

Naveen Babu* and Nameesha Chauhan

Shiv Nadar Institution of Eminence, India

ABSTRACT: The dispersion equation for a rectangular tape helix with four rectangular dielectric support rods was derived using precise boundary conditions and field-restricting functions. The dispersion equation is a simplified conjoint expression obtained for the axial and transverse directions, derived by solving an infinite set of linear homogeneous simultaneous equations, represented as an infinite-order matrix whose determinant is zero. The dispersion characteristics plotted from the simplified dispersion equation consist of dominant and additional higher-order modes, similar to an open rectangular slow-wave structure (SWS), but with the existence of $\beta_0 a(k_0 a)$ roots everywhere without the limitations of the forbidden region boundary. The phase velocity curves obtained for the corresponding mode of the dispersion characteristics exhibit comparable behavior to the free-space rectangular helix SWS, especially in the third "allowed" region, which offers a wider beam-wave interaction region with phase speed equivalent to the speed of light at higher operating frequencies. The numerically computed dispersion curves and their corresponding phase velocities were plotted. Similar dimensional variations of the structure with discrete support rods were simulated using three-dimensional simulation software. The dispersion characteristics obtained from the simplified dispersion equation along with the dimensional variation of the dielectric-loaded rectangular tape helix SWS determine the capability and limitations of such minuscule traveling wave tubes (TWTs) as planar TWTs suitable for fabrication using micro-machining techniques.

1. INTRODUCTION

Traveling wave tubes (TWTs) are rapidly evolving with applications in the 21st century, such as 6G communications, high-resolution radars with expanding functionalities, high-data-rate wireless links, and high-throughput satellite communications. The exploitation of the frequency spectrum by newly developed communication equipment has forced researchers to think beyond GHz frequency ranges and venture into the THz spectrum. Cylindrical TWTs exhibit indisputable dominance, with high power, gain, and bandwidth amplification in the GHz frequency range. With an emphasis on amplification in the extended frequency spectrum in the THz range, conventional cylindrical TWTs have limitations in terms of manufacturing flexibility, cost, performance, and operating frequency range. With the advent of micro-machining techniques such as 3D printing and more advanced research in the field of materials science, it is now possible to fabricate rectangular and planar slow-wave structures (SWSs), including dielectric support structures with required permittivity.

Cold test analysis of unsupported tape-helix cylindrical TWTs using both field [1] and equivalent circuit [2] analysis approaches has been well established. Practically relevant cylindrical tape helices supported by dielectric rods [3] and corrugated dielectric support rods [4–6] have also been reported. Most reported tape-helix SWS models account for the anisotropic conductivity [7] of the tape rather than the perfectly conducting tape model [8, 9] because it is well known that the contribution of the perpendicular component of the surface current density in a perfectly conducting model is negligible and often ignored. The cold test models reported with anisotropic tape material conductivity and dielectric rod support structures were extended to perform a large-signal field analysis in [10].

Field analysis of planar tape TWTs with unidirectional conducting (UC) sheets suspended in vacuum [11, 12] and planar UC sheets enclosed infinitely with dielectric tubes [13] have been reported by earlier researchers. Kumar and Aditya [14] proposed a simplified tape-helix analysis for unloaded SWS with straight edge connections, in which the effective dielectric constant (EDC) method exhibited accurate dispersion beyond the cut-off frequency. The field analysis of a rectangular unloaded planar SWS considering only one-quarter of the structure to satisfy the boundary conditions and dividing the cross-sectional geometry into four regions was proposed by Fu et al. in [15]. A similar field analysis approach was extended to the dielectric loaded planar TWT structure by Fu et al. in [16], where the area between the planar rectangular helix and the outer enclosing conductor is filled with dielectric material with the assumption that the permittivity of the discrete dielectric rods, ϵ_r is averaged to obtain the effective permittivity ϵ_{eff}.

Wei et al. in [17] followed the approach of [15] to derive the dispersion equation for a rectangular tape helix for both open and dielectric-loaded structures. Owing to the symmetry of the structure, the cross-section of the helix was divided into four regions. The fourth region, which is the intersection of regions II and III constituting the corner edge of the helix, was ignored because of the negligible electromagnetic field behav-

---

* Corresponding author: Naveen Babu (naveen.babu@snu.edu.in).

doi:10.2528/PIERM23102604

Published by THE ELECTROMAGNETIC ACADEMY

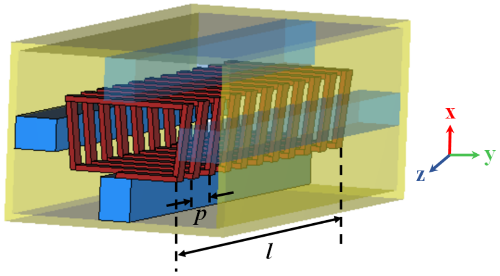

FIGURE 1. Dielectric loaded multi-turn rectangular tape helix structure.

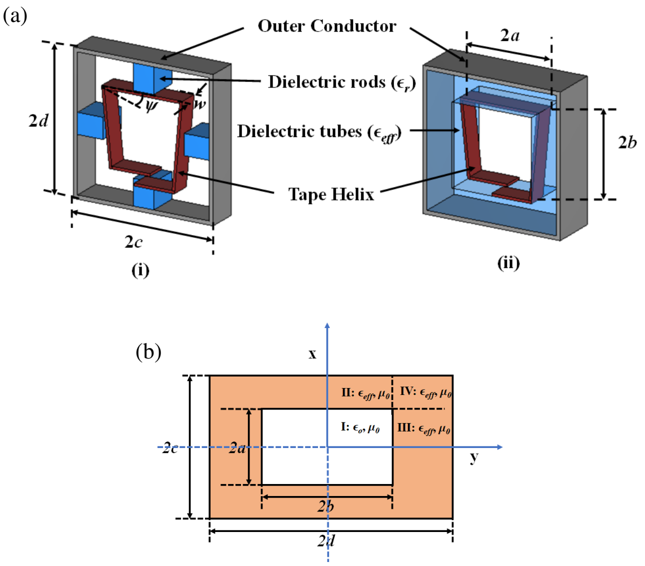

FIGURE 2. Dielectric loaded rectangular tape helix structure. (a) Lateral view with (i) discrete dielectric rods and (ii) smoothened dielectric tubes. (b) Cross-sectional view.

ior at the edges described by Meixner [18]. The distinct aspect of this study arises from the employment of the field confinement function in conjunction with rigorous mathematical manipulation of the appropriate boundary conditions to obtain a refined simplified dispersion equation. This equation not only conforms to the asymptotic behaviors exhibited by its individual components, but also emerges through the precise substitution of complex constant variables at the boundary conditions $x = a$ and $y = b$. In this approach, the dielectric rod permittivity, ϵ_r, is weighted averaged to obtain the effective permittivity ϵ_{eff} calculated using the effective dielectric method (EDC) proposed in [14].

In the first part of this study, a simplified dispersion equation, which is a conjoint expression for $\hat{x}$ and $\hat{y}$ directions was derived using an additional boundary condition that employed a confinement function. The derived dispersion equation was an asymptotically rapidly converging expression of the order $O \sim 1/|n|^2$ which exhibited faster computation for the convergence of the $\beta_0 a(k_0 a)$, $\beta_0 a > 0$ roots. It was also pointed out that the authors in [17] were unable to numerically compute the derived complex dispersion equation for higher-order modes owing to the complexity of the derived dispersion equation; they chose to compute only the fundamental mode by degenerating the dispersion equation for $n = 0$. In this study, the theory proposed for a open rectangular tape helix SWS was extended to a dielectric-loaded rectangular tape helix SWS. Wei et al. [17] derived the dispersion equation for the dielectric-loaded case of planar TWT, but the complexity of the derived dispersion equation was multi-fold, and dispersion characteristics were not computed and ignored. In this study, the electromagnetic field equations were substituted into the accurate field-restricted rectangular tape helix boundary condition and carefully manipulated to obtain the dispersion equation. The dispersion equation thus obtained is much simpler than [17] but more intricate than the open planar TWT structure and is computable with a faster convergence factor for $\beta_0 a$ roots. The dispersion characteristics were plotted from the derived dispersion equation for the dielectric-loaded case, and the corresponding phase velocity was numerically computed. The effects of dimensional variations on the phase velocities and interaction impedances were simulated using CST.

This manuscript contains four sections. Section 2 describes the "problem formulation" of the dielectric-loaded rectangular tape helix SWS, which includes various definitions and dimensions adapted in this study. In addition, this section discusses the field equations in the two regions, boundary conditions, and derivation of the dispersion equation. Section 3, "Results and Discussion", describes the reckoning of the dispersion equation to obtain the dispersion characteristics and simulation plots for the phase velocities and interaction impedance using the three-dimensional electromagnetic simulation tool CST for dimensional variations. Section 4 presents the concluding section that summarizes the findings presented in this paper and provides suggestions for future work.

2. PROBLEM FORMULATION

We use the rectangular tape helix slow-wave structure model described in the open rectangular planar tape helix (PTH) model, except that the structure is now supported by dielectric rods. Accordingly, the loaded tape helix SWS has the dimensions of infinite length l, width of the tape w, pitch angle ψ, pitch p, and infinitesimally thin tape thickness $\delta(\downarrow 0)$, as shown in Figs. 1 and 2(a). To maintain uniformity, the notations and definitions in this study are the same as those used in the open rectangular PTH model. The rectangular tape helix had a height of $2a$ and width of $2b$, and the height and width of the complete structure, including the dielectric rods and outer conductor, were $2c$ and $2d$, respectively. The axis of the rectangular tape helix was along the $\hat{z}$ coordinate of the rectangular Cartesian coordinate system $(\hat{x}, \hat{y}, \hat{z})$. Henceforth, equations and expressions referring to the open rectangular PTH model are referenced with Prefix I in this manuscript. The dielectric-loaded tape helix is further approximated to be lossless, with dielectric rods providing complete insulation between the tape and the outer conductor; the tape conductivity is anisotropic and lossless. The structure exhibits periodicity such that $f(x, y, z) = f(x \pm a, y, z) = f(x, y \pm b, z)$, and accordingly, both even and odd propagating modes exist. In this analysis, only odd modes corresponding to the transverse antisymmetric mode of propagation were considered.

From the lateral view of the rectangular tape helix shown in Fig. 2(a)-(ii), the tape helix is supported by four rectangular dielectric support rods with permittivity ϵ_r. The tape helix and dielectric rods are enclosed within the outer conductor. For simplicity, the discrete dielectric support rods are smoothed to fill the gap region between the tape and outer conductor, thereby forming a dielectric tube or an enclosure between the tape helix and outer conductor. The permittivity, ϵ_r of the dielectric rods after smoothing is weighted averaged out to obtain the effective permittivity, ϵ_{eff} of the dielectric tube using the EDC method proposed in [14] as shown in Fig. 2(a). In this analysis, only one-quarter of the structure governed by the limits mentioned below was considered for the sake of simplicity. The cross-sectional structure is divided into four regions as shown in Fig. 2(b) with the following dimensional limits: (a) Region I (vacuum): $(0 < x \leq a$ and $0 < y \leq b)$; (b) Region II (dielectric): $(a < x \leq c$ and $0 < y \leq b)$; (c) Region III (dielectric): $(0 < x \leq a$ and $b < y \leq d)$; and (d) Region IV (dielectric): $(a < x \leq c$ and $b < y \leq d)$. Region IV is usually ignored because of the weak fields in the corner regions, as per Meixner [18] and Marcatili [19]. Therefore, only the field equations corresponding to regions I–III were considered for the analysis.

2.1. Field Equations

The eigen-functions in the Cartesian coordinate system for the electric and magnetic fields can be obtained from the Vector Helmholtz wave equation. The fields have periodic symmetricity with simultaneous rotation and translation with respect to the wave propagating $+z$ direction, defined as $e^{(j\omega t - \beta_n z)} \underline{\triangle}\, e^{j\varphi}$, where ω is the angular frequency, and β_n is the propagating field constant. Hence, following Floquet's theorem, the electromagnetic field equations are represented as the sum of an infinite series of rectangular harmonics obtained from the scalar wave equation using the method of separation of variables.

$$\frac{\partial^2 \phi}{\partial x^2} + \frac{\partial^2 \phi}{\partial y^2} = \tau_n^2 \phi \ \text{ for } \ 0 < x \leq a \text{ and } 0 < y \leq b \quad \text{(1a)}$$

$$\frac{\partial^2 \phi}{\partial x^2} + \frac{\partial^2 \phi}{\partial y^2} = \tau_n^{+2} \phi \ \text{ for } \ a < x \leq c \text{ and } b < y \leq d \quad \text{(1b)}$$

where $\phi = E$ or H, $\tau_n^2 = \beta_n^2 - k_0^2 = \tau_{xn}^2 + \tau_{yn}^2$, and $\tau_n^{+2} = \beta_n^2 - \epsilon_0 \epsilon_{\mathit{eff}} k_0^2 = \tau_{xn}^{+2} + \tau_{yn}^{+2}$. The "+" in the superscript of τ_n, $n \in \mathbb{Z}$ denotes the transverse wave number in the dielectric tube region $(a < x \leq c$ and $b < y \leq d)$. $\beta_n \underline{\triangle}\, \beta_0 + 2\pi n/p$, where $\beta_0 = \beta(\omega)$ is the fundamental guided wave propagation constant for nth space harmonic of electromagnetic waves supported by the dielectric-loaded rectangular tape helix SWS at radian frequency ω, and τ_{xn} and τ_{yn} are the propagation coefficients in the x and y directions, respectively. The free-space wave number at the radian frequency ω is defined as $k_0 \underline{\triangle}\, \omega/c$, where c is the velocity of light given as $c = 1/\sqrt{\mu_0 \epsilon_0}$. The free space permeability and permittivity are μ_0 and ϵ_0, respectively. With the aforementioned definitions, it is now possible to formulate tangential field expressions using the method of separation of variables. Accordingly, the field equations in various regions are as follows:

- Region I $(0 < x < a)$ and $(0 < x < b)$

$$E_{1z} = \sum_{n=-\infty}^{\infty} A_n^* \cosh[\tau_{1xn} x] \cosh[\tau_{1yn} y] \mathrm{e}^{jn\varphi} \quad (2)$$

$$H_{1z} = \sum_{n=-\infty}^{\infty} B_n^* \cosh[\tau_{1xn} x] \cosh[\tau_{1yn} y] \mathrm{e}^{jn\varphi} \quad (3)$$

- Region II $(a < x \leq c$ and $0 < y \leq b)$

$$E_{2z} = \sum_{n=-\infty}^{\infty} C_n^* \cosh[\tau_{2xn}(c - x)] \cosh[\tau_{2yn} y] \mathrm{e}^{jn\varphi} \quad (4)$$

$$H_{2z} = \sum_{n=-\infty}^{\infty} D_n^* \cosh[\tau_{2xn}(c - x)] \cosh[\tau_{2yn} y] \mathrm{e}^{jn\varphi} \quad (5)$$

- Region III $(0 < x \leq a$ and $b < y \leq d)$

$$E_{3z} = \sum_{n=-\infty}^{\infty} E_n^* \cosh[\tau_{3xn} x] \cosh[\tau_{3yn}(d - y)] \mathrm{e}^{jn\varphi} \quad (6)$$

$$H_{3z} = \sum_{n=-\infty}^{\infty} F_n^* \cosh[\tau_{3xn} x] \cosh[\tau_{3yn}(d - y)] \mathrm{e}^{jn\varphi} \quad (7)$$

- Region IV $(a < x \leq c$ and $b < y \leq d)$

$$\begin{aligned} E_{4z} &= \sum_{n=-\infty}^{\infty} G_n^* \sinh[\tau_{4xn}(c - x)] \\ &\quad \times \sinh[\tau_{4yn}(d - y)] \mathrm{e}^{jn\varphi} \qquad (8) \\ H_{4z} &= \sum_{n=-\infty}^{\infty} H_n^* \cosh[\tau_{4xn}(c - x)] \\ &\quad \times \cosh[\tau_{4yn}(d - y)] \mathrm{e}^{jn\varphi} \qquad (9) \end{aligned}$$

where τ_{ixn} and τ_{iyn} for $i = 1$ to 4 in (2)–(9) are the propagation coefficients in the x and y directions in regions I–IV, respectively. Also, $\tau_{1xn} = \tau_{xn}$, $\tau_{1yn} = \tau_{yn}$, $\tau_{2xn} = \tau_{3xn} = \tau_{4xn} = \tau_{xn}^+$ and $\tau_{2yn} = \tau_{3yn} = \tau_{4yn} = \tau_{yn}^+$. In (2)–(9), A_n^*, B_n^*, C_n^*, D_n^*, E_n^*, F_n^*, G_n^*, and H_n^* are the constants of the field coefficients to be determined for the dielectric-loaded rectangular tape helix SWS case by substituting in the boundary conditions covered in the next subsection. The other field equations in regions II–IV can be generalized as

$$E_{ix} = \frac{j\beta_n}{W_n^2}\frac{\partial E_{iz}}{\partial x} + \frac{j\omega\mu_0}{W_n^2}\frac{\partial H_{iz}}{\partial y} \tag{10a}$$

$$E_{iy} = \frac{j\beta_n}{W_n^2}\frac{\partial E_{iz}}{\partial y} - \frac{j\omega\mu_0}{W_n^2}\frac{\partial H_{iz}}{\partial x} \tag{10b}$$

$$H_{ix} = -\frac{j\omega\epsilon_0\epsilon_{\mathit{eff}}}{W_n^2}\frac{\partial E_{iz}}{\partial y} + \frac{j\beta_n}{W_n^2}\frac{\partial H_{iz}}{\partial x} \tag{10c}$$

$$H_{iy} = \frac{j\omega\epsilon_0\epsilon_{\mathit{eff}}}{W_n^2}\frac{\partial E_{iz}}{\partial x} + \frac{j\beta_n}{W_n^2}\frac{\partial H_{iz}}{\partial y} \tag{10d}$$

where $i = 1$ to 4 indicates the region of the rectangular tape helix. In (10),

$$W_n^2 = \begin{cases} \tau_n^2 & \text{for } i = 1 \\ \tau_n^{+2} & \text{for } i = 2\text{–}4 \end{cases}$$

It is to be reiterated that the field representations corresponding to region IV are ignored owing to the weak fields present in the corner edges of the structure that do not contribute significantly to the analysis; rather, this assumption simplifies the problem approach in determining the dispersion equation.

2.2. Boundary Conditions

For the cross-sectional structure shown in Fig. 2(b) for a rectangular tape helix supported by a dielectric tube enclosed by an outer conductor, the boundary conditions along x and y directions are as follows:

I. *The electric field boundary conditions are*

- The tangential electric fields along $\hat{z}$ directions are continuous for all values of z.
- The tangential electric field along $\hat{y}$ direction disappears on the tape surface.
- The tangential electric field along $\hat{x}$-direction disappears on the tape surface.

Thus, at $(x = a, -b \le y \le b)$,

$$E_{1z}(a-, y, z) - E_{2z}(a+, y, z) = 0 \tag{11a}$$

$$E_{1y}(a-, y, z) - E_{2y}(a+, y, z) = 0 \tag{11b}$$

$$[E_{2z}\sin\psi - E_{2y}\cos\psi]\, g(y, z) = 0 \tag{11c}$$

and at $(-a \le x \le a, y = b)$

$$E_{1z}(x, b-, z) - E_{3z}(x, b+, z) = 0 \tag{11d}$$

$$E_{1x}(x, b-, z) - E_{3x}(x, b+, z) = 0 \tag{11e}$$

$$[E_{3z}\sin\psi - E_{3x}\cos\psi]\, g(x, z) = 0 \tag{11f}$$

II. *The magnetic field boundary conditions is*

- The magnetic field discontinuity along the propagating $\hat{z}$ direction is equal to the surface current density components, as given below:

Thus at $(x = a, -b \le y \le b)$,

$$H_{1z}(a-, y, z) - H_{2z}(a+, y, z) = J_y|_{x=a} \tag{12a}$$

$$H_{1y}(a-, y, z) - H_{2y}(a+, y, z) = -J_z|_{x=a} \tag{12b}$$

and at $(-a \le x \le a, y = b)$

$$H_{1z}(x, b-, z) - H_{3z}(x, b+, z) = -J_x|_{y=b} \tag{12c}$$

$$H_{1x}(x, b-, z) - H_{3x}(x, b+, z) = J_z|_{y=b} \tag{12d}$$

In (11) and (12), the tape helix region inside the helix filled with vacuum is represented as $(a-, b-)$, and the region outside the helix filled with dielectric is represented as $(a+, b+)$. The surface current density components in (12) along $\hat{x}$, $\hat{y}$, and $\hat{z}$ directions are represented as J_x, J_y, and J_z, respectively. The confinement boundary conditions are expressed as (11c) and (11f), respectively, where functions $g(x, z)$ and $g(y, z)$ are the confinement functions introduced to restrict the tangential electric field to zero on the tape surface. The confinement functions are defined as follows:

$$g(x, z) \underline{\triangle} \sum_{l=-\infty}^{\infty} 1_{I_l(x)}(z), \text{ within the interval}$$

$$\{z|(l + y/p) - w/2 \le z \le (l + y/p) + w/2\}$$

$$g(y, z) \underline{\triangle} \sum_{l=-\infty}^{\infty} 1_{I_l(y)}(z), \text{ within the interval}$$

$$\{z|(l + x/p) - w/2 \le z \le (l + x/p) + w/2\}$$

2.3. Surface Current Density Expansions and Dispersion Equation

For the anisotropic conductivity of the tape helix, the perpendicular component of the surface current density, $J_\perp = 0$, and the total surface current density, $J_s = J_\|$ at helix boundaries $x = a$ and at $y = b$. The parallel component of the surface current density is governed by the functional dependence of the variables x and y along z due to the symmetry and periodicity imposed by the tape helix geometry. Hence, $J_\|(x, z)|_{x=a} = J_\|(y, z)|_{y=b}$. Accordingly, $J_\|(x, z)|_{x=a}$ and $J_\|(y, z)|_{y=b}$ are defined as follows:

$$J_\|(x, z)|_{x=a} = \left(\sum_{n\in\mathbb{Z}} J_n e^{-j\beta_n z}\right) g(x, z)|_{x=a} \tag{13a}$$

$$J_\|(y, z)|_{y=b} = \left(\sum_{n\in\mathbb{Z}} J_n e^{-j\beta_n z}\right) g(y, z)|_{y=b} \tag{13b}$$

where the nth space harmonic Fourier coefficients of the surface current density, J_n, are given by

$$J_n = \int_{-w/2}^{+w/2} J_0 e^{-j(\beta_0 z - \beta_n z)} dz = J_0 \operatorname{sinc}\left(\frac{n\pi w}{2}\right) \tag{14}$$

where J_0 represents an undetermined constant amplitude assumed to flow along the tape helix winding path approximated by a narrow, anisotropic conducting tape. The confinement functions $g(x,z)$ and $g(y,z)$ on the right-hand side of (13) ensure that the surface current density is confined within the tape surface only, and not elsewhere. In (14),

$$\mathrm{sinc}_\pi(X) \equiv \mathrm{sinc}(\pi X) = \begin{cases} \frac{\sin \pi X}{\pi X} & \text{if } X \neq 0 \\ 1 & \text{if } X = 0 \end{cases} \tag{15}$$

For a given pitch angle ψ, from the geometry of the tape helix structure, the following winding direction surface current density components are resolved as given below [17] in the axial and orthogonal directions with $J_\perp = 0$

$$J_y|_{x=a} = J_{||} \cos\psi = \sum_{n\in\mathbb{Z}} J_{yn}\, \mathrm{e}^{-j\beta_n z} \tag{16a}$$

$$J_z|_{x=a} = J_{||} \sin\psi = \sum_{n\in\mathbb{Z}} J_{zn}\, \mathrm{e}^{-j\beta_n z} \tag{16b}$$

$$J_x|_{y=b} = -J_{||} \cos\psi = \sum_{n\in\mathbb{Z}} J_{xn}\, \mathrm{e}^{-j\beta_n z} \tag{16c}$$

$$J_z|_{y=b} = J_{||} \sin\psi = \sum_{n\in\mathbb{Z}} J_{zn}\, \mathrm{e}^{-j\beta_n z} \tag{16d}$$

We can now address the boundary conditions using the preceding definitions. Taking into account the following approximation of the ratio of the propagation coefficients that determine the mode number of propagation in a rectangular waveguide:

$$\frac{\tau_{i\gamma n}}{\tau_{j\gamma n}} = 1 \tag{17}$$

where i, j correspond to the region of the tape cross-section that can take values from 1–3, provided that $i \neq j$ and γ correspond to the directions x or y; within the bounds of the anticipated wave propagation in the rectangular waveguide structure, the aforementioned approximation holds true. By substituting the electric field expressions given in (2)–(10b) into the electric field boundary conditions in (11), we obtain the following field constants in terms of the field constants A_n^* or B_n^*

$$C_n^* = A_n^* \left[\frac{\cosh(\tau_{xn}a)}{\sinh(\tau_{xn}(c-a))}\right] \tag{18a}$$

$$E_n^* = A_n^* \left[\frac{\cosh(\tau_{yn}b)}{\sinh(\tau_{yn}(d-b))}\right] \tag{18b}$$

$$D_n^* = -B_n^* \left(\frac{\tau_n^{+2}}{\tau_n^2}\right) \left[\frac{\sinh(\tau_{xn}a)}{\sinh(\tau_{xn}(c-a))}\right] \tag{18c}$$

$$F_n^* = -B_n^* \left(\frac{\tau_n^{+2}}{\tau_n^2}\right) \left[\frac{\sinh(\tau_{yn}b)}{\sinh(\tau_{yn}(d-b))}\right] \tag{18d}$$

Similarly, satisfying the magnetic field boundary conditions in (12) using the magnetic field expressions in (3)–(10d) together with the field constant expressions in (18), from (12a) and (12b) at $x = a$,

$$B_n^*|_{x=a} = \left[\frac{J_0 \tau_{yn}}{2}\right] \times \left[\frac{\mathrm{csch}(\tau_{yn}b)}{\sinh(\tau_{xn}a)}\right] \left[\frac{\cos\psi\, \mathrm{sinc}\left(\frac{n\pi w}{p}\right)}{\xi_{na}}\right] \tag{19a}$$

$$A_n^*|_{x=a} = j\left[\frac{J_0}{2\omega\epsilon_0\epsilon_{\mathit{eff}}}\right]\left[\frac{\tau_{yn}}{\tau_{xn}}\right] \times \left[\frac{\mathrm{csch}(\tau_{yn}b)}{\cosh(\tau_{xn}a)}\right]\left[\frac{\tau_n^{+2} \sin\psi\, \mathrm{sinc}\left(\frac{n\pi w}{p}\right)}{\chi_{na}}\right] \tag{19b}$$

Thus, all field constants $A_n^*, B_n^*, C_n^*, D_n^*, E_n^*$, and F_n^* are obtained from the boundary conditions listed in (11) to (12b). However, it is obligatory to satisfy all the magnetic boundary conditions in (12), despite determining all the field constants. It can be observed from (18) and (19) that the field constant A_n is complex, and therefore, C_n^* and E_n^* are also complex, whereas B_n^*, D_n^*, and F_n^* are non-complex field constants. Another set of field constants for A_n^* and B_n^* may be resolved in a manner similar to that detailed in the open rectangular PTH model by simply swapping the propagation coefficients $\tau_{yn}b$ with $\tau_{xn}a$ and vice versa, or by satisfying the boundary conditions in (12c) and (12d). Thus, using the field constants in (18) and satisfying the magnetic field boundary conditions in (12c) and (12d) evaluated at $y = b$, we obtain:

$$B_n^*|_{y=b} = \left[\frac{J_0 \tau_{xn}}{2}\right] \times \left[\frac{\mathrm{csch}(\tau_{xn}a)}{\cosh(\tau_{yn}b)}\right] \left[\frac{\cos\psi\, \mathrm{sinc}\left(\frac{n\pi w}{p}\right)}{\xi_{nb}}\right] \tag{20a}$$

$$A_n^*|_{y=b} = j\left[\frac{J_0}{2\omega\epsilon_0\epsilon_{\mathit{eff}}}\right]\left[\frac{\tau_{xn}}{\tau_{yn}}\right] \times \left[\frac{\mathrm{csch}(\tau_{xn}a)}{\cosh(\tau_{yn}b)}\right]\left[\frac{\tau_n^{+2} \sin\psi\, \mathrm{sinc}\left(\frac{n\pi w}{p}\right)}{\chi_{nb}}\right] \tag{20b}$$

where in (19) and (20),

$$\chi_{na} = \coth(\tau_{xn}a)\coth(\tau_{xn}(c-a)) + \left[\frac{\tau_n^{+2}}{\tau_n^2}\right] \tag{21a}$$

$$\chi_{nb} = \coth(\tau_{yn}b)\coth(\tau_{yn}(d-b)) + \left[\frac{\tau_n^{+2}}{\tau_n^2}\right] \tag{21b}$$

$$\xi_{na} = \coth(\tau_{xn}a) + \left[\frac{\tau_n^{+2}}{\tau_n^2}\right]\coth(\tau_{xn}(c-a)) \tag{21c}$$

$$\xi_{nb} = \coth(\tau_{yn}b) + \left[\frac{\tau_n^{+2}}{\tau_n^2}\right]\coth(\tau_{yn}(d-b)) \tag{21d}$$

On equating (19) and (20), the ratio of the wave propagation coefficients is given as

$$\left(\frac{\tau_{yn}}{\tau_{xn}}\right)^2 = \frac{\coth(\tau_{xn}a)\coth(\tau_{xn}(c-a)) + \left[\frac{\tau_n^{+2}}{\tau_n^2}\right]}{\coth(\tau_{yn}b)\coth(\tau_{yn}(d-b)) + \left[\frac{\tau_n^{+2}}{\tau_n^2}\right]} \tag{22}$$

The aforementioned ratio is expressed in terms of established quantities. It is then substituted into the field constant expressions to determine the roots of the dispersion equation. The final boundary condition is a conjoint expression derived from (11c) evaluated at $x = a$ in the interval $-b \leq y \leq b$ and (11f) evaluated at $y = b$ in the interval $-a \leq x \leq a$. The presence of confinement functions ensures that the current density is restricted to the tape surfaces. This leads to the following representation of the final boundary condition.

$$\left(\int_{-b}^{b} \left[E_{2z}|_{x=a} \sin\psi - E_{2y}|_{x=a} \cos\psi\right] g(y,z)dy \right.$$
$$\left. + \int_{-a}^{a} \left[E_{3z}|_{y=b} \sin\psi - E_{3x}|_{y=b} \cos\psi\right] g(x,z)dx \right) = 0 \quad (23)$$

Using the relevant field constants corresponding to the electric field expressions evaluated at appropriate boundaries and intervals, the dispersion equation for the dielectric-loaded rectangular tape helix can be derived from (23). For instance, the field expressions E_{2z} and E_{2y} are evaluated at $x = a$ in the interval $-b \leq y \leq b$, using the field constants C_n^* and D_n^* which in turn use A_n^* and B_n^* obtained from (19). Similarly, the field expressions E_{3z} and E_{3x} are evaluated at $y = b$ in the interval $-a \leq y \leq a$, employing the field constants E_n^* and F_n^* which, in turn, use the field constants A_n^* and B_n^* derived in (20). With certain judicious algebraic manipulations, we can formulate the following dispersion equation:

$$j \frac{\tau_n^2 J_0}{\omega \epsilon_0 \epsilon_{eff}} \operatorname{sinc}\left(\frac{n\pi w}{p}\right) \sum_{n\in\mathbb{Z}} \sum_{l\in\mathbb{Z}} \left\{ \left[\left(\frac{e^{-\tau_{xn} a} \sigma'_{xn} a}{\tau_{xn}} \right) 1_{I_l(x)}(z) \right.\right.$$
$$\left.\left. + \left(\frac{e^{-\tau_{yn} b} \sigma'_{xn} b}{\tau_{yn}} \right) 1_{I_l(y)}(z) \right] \right\} = 0 \quad (24)$$

where

$$\begin{bmatrix} \sigma'_{xn} a \\ \sigma'_{xn} b \end{bmatrix} = \begin{bmatrix} \frac{(\tau_n^+/\tau_n)^2}{\chi_{na}} & \frac{\tau_{xn}^2}{\tau_n^4} \frac{k_0^2}{\xi_{na}} \\ -\frac{(\tau_n^+/\tau_n)^2}{\chi_{nb}} & \frac{\tau_{yn}^2}{\tau_n^4} \frac{k_0^2}{\xi_{nb}} \end{bmatrix} \begin{bmatrix} \sin^2\psi \\ \cos^2\psi \end{bmatrix}$$

where χ_{na}, χ_{nb}, ξ_{na}, and ξ_{nb} are defined by (21). Owing to the use of the confinement function across the tape surface for wave propagation along the $+z$ direction, the deduced dispersion equation for the dielectric-supported rectangular tape helix TWT is more precise and simple than the dispersion equation provided in [17]. Thus, the dispersion equation is evidently reliable for the following two reasons: (a) When the limiting constraints imposed by the impact of dielectric loading are applied to the dispersion equation (24), it is shown to degenerate to the dispersion equation for the open rectangular planar tape helix (PTH) case by only allowing $\epsilon_{eff} \to 1$; (b) The dispersion equations in open planar tape helix and (24) are identical and equivalent.

In (24), $e^{-\tau_{xn} a} \neq 0$ and $e^{-\tau_{yn} b} \neq 0$ which implies that the Fourier coefficients must vanish. Thus, using (14), dispersion equation (24) becomes

$$\sum_{n\in\mathbb{Z}} J_0 \left(\sigma'_{xn} a + \sigma'_{yn} b\right) \operatorname{sinc}\left(\frac{n\pi w}{p}\right) = 0 \quad (25)$$

To obtain a more generalized representation of the infinite set of homogeneous simultaneous equations, the Fourier coefficient of the surface current density component J_0 in (25) must be replaced with the resolved current density components from (16) based on the direction and region of operation. However, because of the nature of the direction-specific variables of the surface current density components, the resolved current density parameters can be specified generically as the winding direction component of the surface current density as $J_{||}$ and (25) can be represented as

$$\sum_{j\in\mathbb{Z}} \alpha_{ij} J_{||j} = 0 \quad \text{for } i \in \mathbb{Z} \quad (26)$$

where

$$\alpha_{ij} = \sum_{n\in\mathbb{Z}} \left(\sigma'_{xn} a + \sigma'_{yn} b\right)$$
$$\times \operatorname{sinc}\left[\frac{(i-n)\pi w}{p}\right] \operatorname{sinc}\left[\frac{(j-n)\pi w}{p}\right] \quad (27)$$

In (26), α_{ij} is an $i \times j$ matrix of infinite order, and $J_{||j}$ is the column matrix of size $j \times 1$. This study places heavy emphasis on the idea of field confinement within the tape surface, and the existence of the sinc function in (27) in every coefficient element of the matrix α_{ij} realizes the field restriction. For a justifiable solution of (26), the infinite-order matrix α_{ij} must be truncated to a finite order, and the determinant of the coefficient matrix $|\mathbf{A}| \underline{\triangle} \alpha_{ij}$ must be zero, that is,

$$|\mathbf{A}| = 0 \quad (28)$$

Thus, theoretically, (28) is the simplified dispersion relation for the dielectric-supported rectangular tape helix SWS enclosed by an outer conductor, with the tape material having anisotropic conductivity.

2.4. Interaction Impedance

The interaction impedance for the nth space harmonic of a periodic slow wave structure can be expressed as in [20].

$$\eta_n = \frac{|E_{zn}|^2}{2P_{av}\beta_n^2} \quad (29)$$

where P_{av} is the time-averaged RF power determined from E_{iz}, $i = 1$–4 expressed as in (10).

3. NUMERICAL COMPUTATION AND SIMULATION

Using α_{ij} in (26), the numerical computation of the dispersion equation can be performed using various dimensional and computational parameters as described below. Upon observing $\sigma'_{xn} a$ and $\sigma'_{yn} b$ in (24), the asymptotic behavior of the dispersion equation is of the order $O \sim 1/|n|^2$, and the convergence of the roots for $\beta_0 a(k_0 a)$ is anticipated to be faster and decisively satisfactory for the desired accuracy. The dispersion curve is plotted for pitch angle, $\psi = 10°$, effective permittivity, $\epsilon_{eff} = 1.34$, dimensional ratios, $w/p = 0.33$ (a narrow tape), $b/a = 1$ with $a = 1.17$ mm, and $c/d = 1$ with $c = 1.872$ mm.

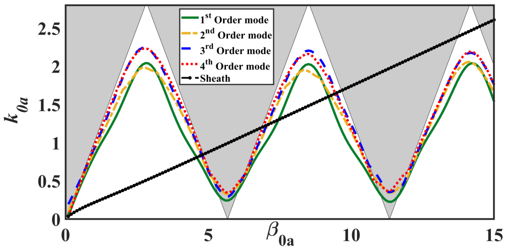

FIGURE 3. Numerically computed dominant and higher-order mode dispersion characteristics of a dielectric-loaded rectangular tape helix slow-wave structure and sheath helix structure.

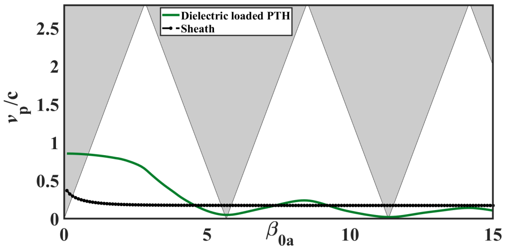

FIGURE 4. Numerically computed phase velocity plot corresponding to the dominant mode dispersion characteristics of a dielectric loaded rectangular tape helix slow-wave structure.

A dispersion coefficient matrix of order $N = 10$ was considered, with each entry of the matrix undergoing convergence iterations for $M = 30$. However, it was observed during the computation that the convergence of all coefficients up to a decimal accuracy of 0.0001 occurred for $M \leq 15$. Despite forcing each coefficient of the dispersion matrix to iterate 30 times and computing the matrix of order 10×10, the computation time for the complete dispersion plot was less than 80 s on a 3.30 GHz processor for all values of $\beta_0 a$ ranging from 1 to 16 with an incremental step size of $\Delta\beta_0 a = 0.1$. This drastic reduction in the computation time would not have been possible without proper manipulation in the derivation of the dispersion equation, which includes approximations such as in (17), the inclusion of additional confinement functions, and mathematical maneuvers of variables as produced in (24).

The dispersion curve between $\beta_0 a$ and $k_0 a$ is plotted in Fig. 3, and it is worth emphasizing that the dispersion characteristics for a dielectric-loaded rectangular tape helix have not been reported in the literature and resemble the dispersion plot for a dielectric-loaded cylindrical tape helix presented in [3]. In Fig. 3, the fundamental mode dispersion characteristics, along with the three higher-order modes, are plotted in comparison with the theoretical sheath model of the tape helix. The triangular boundaries and shaded "forbidden" regions are notional for this model and are reproduced for the sake of comparison with the previous open tape helix model. The roots of the dispersion equation for the dielectric-loaded model are unbound and can exist everywhere in the $\beta_0 a - k_0 a$ space. The dispersion plot for the dielectric-loaded rectangular tape helix is no longer an approximation for the dielectric-loaded sheath model of the tape helix for a given ϵ_{eff}.

The fundamental mode of the dispersion plot starts closer to zero for small values of $\beta_0 a \geq 0$ whereas higher-order modes have a significant $k_0 a$ value. The plots of all higher-order modes are similar to that of the fundamental mode; hence, the analysis here is performed with respect to the fundamental mode only. The higher-order modes throughout the plot remain higher than the fundamental mode, except for the second-order mode, which overlaps the fundamental mode at the peak values in the first, second, and third "allowed" regions. The fundamental mode dispersion characteristics increased with an increase in $\beta_0 a$ and started decreasing after reaching a peak value at $\beta_0 a = 2.5$. The decreasing plot of the fundamental mode for values of $\beta_0 a \approx 5.5$ enters the notional "forbidden region" and again starts increasing in the second "allowed" region. This pattern is observed in the first "allowed" region and repeats in the second and third "allowed" regions. In the third "allowed" region, the dispersion curve of the dielectric-loaded rectangular tape helix remains below that of the sheath helix model. It is worth emphasizing that the presented dispersion plot was obtained only after allowing the roots to undergo quadratic weighted linear regression smoothing. The phase speed curve for the rectangular dielectric-loaded tape helix model corresponding to the fundamental mode of the dispersion characteristics is shown in Fig. 4. The usable flat region of operation for the electron beam interaction leading to the possible large signal amplification of the rectangular TWTs corresponds to $0.1 \leq \beta_0 a \leq 2.8$ and $14 \leq \beta_0 a \leq 14.4$. The flat portion of the plot corresponding to the roots $0.1 \leq \beta_0 a \leq 2.8$ produces a phase velocity output equal to 76%–80% of the velocity of the light and is hence not desirable for signal amplification. However, the second flat region of the plot, corresponding to $14 \leq \beta_0 a \leq 14.4$, produces a phase velocity of 14.58% of the velocity of light and is a desirable region of operation for signal amplification. In the same region, the rectangular tape helix exhibited superior operation compared to the sheath model, which produced a phase velocity of 17.38% of the velocity of light.

Using the eigenmode solver in the 3D simulation tool CST, a simulation of the rectangular periodic structure with perfect electric conductor (PEC) tape material supported with four discrete rectangular dielectric rods made of email1 with a relative permittivity, $\epsilon_r = 5.1$, is carried out. The dielectric material is enclosed by an outer conductor, as shown in Fig. 2. The structure was simulated to obtain the phase velocity and interaction impedance plots for $b/a = 1, 2, 4$ and 10, with dimensions "a" taking values of 15.85 mm, 1.17 mm, 0.058 mm, and 0.232 mm, respectively. Appropriate boundary conditions were applied to the structure to simulate the desired operating-frequency ranges, as shown in Figs. 5–8. Comparing the simulated plots in this work with the open rectangular tape helix structure, the phase velocity values of the dielectric-loaded structure are approximately 50% less than the phase velocity values simulated in the open rectangular tape structures. As can be seen from the plots in Figs. 5–8, the operational frequency ranges expand as the dimensions decrease, reaching far into the THz frequency ranges. From the simulation plots, we can deduce that THz-frequency operation is feasible for small-

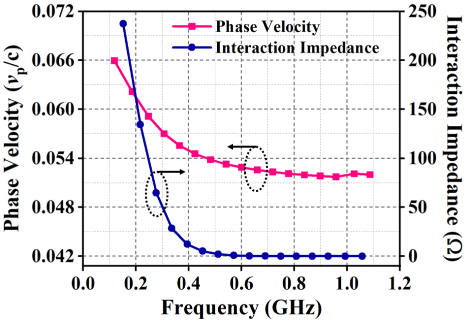

FIGURE 5. Simulated curves of phase velocity and interaction impedance for a dielectric-loaded rectangular tape helix slow wave structure with $b/a = 1$, $\psi = 10°$, $a = 15.85$ mm.

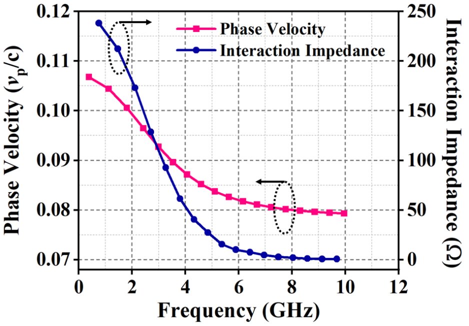

FIGURE 6. Simulated curves of phase velocity and interaction impedance for a dielectric-loaded rectangular tape helix slow wave structure with $b/a = 2$, $\psi = 10°$, $a = 1.17$ mm.

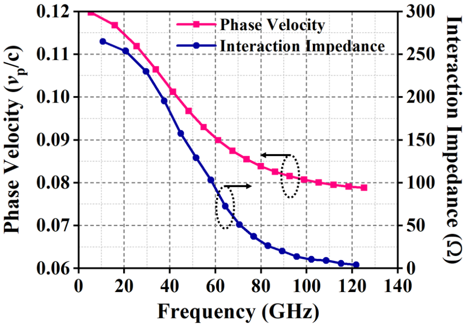

FIGURE 7. Simulated curves of phase velocity and interaction impedance for a dielectric-loaded rectangular tape helix slow wave structure with $b/a = 4$, $\psi = 10°$, $a = 0.058$ mm.

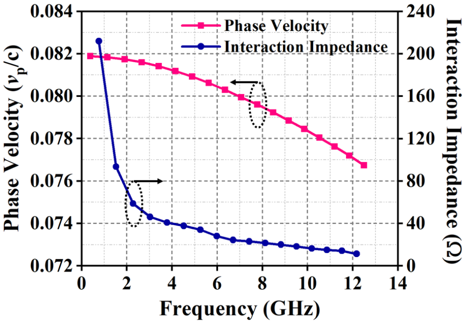

FIGURE 8. Simulated curves of phase velocity and interaction impedance for dielectric-loaded rectangular tape helix slow wave structure with $b/a = 10$, $\psi = 10°$, $a = 0.232$ mm.

dimensional rectangular SWS if such SWS can be manufactured using state-of-the-art printing techniques.

4. CONCLUSION

This study derives a simplified yet accurate dispersion equation and plots the dispersion characteristics and phase velocity plots for a practically relevant dielectric-loaded rectangular tape helix slow-wave structure. A simplified dispersion equation was derived by incorporating confinement functions into the boundary conditions. The derived dispersion equation was plotted for dispersion characteristics with fundamental and higher-order modes. In future work, the effects of additional dimensional variations of the model can be investigated, and a large-signal field analysis of the rectangular tape helix with a sheet beam can be used to calculate the output power, gain, and efficiency. In subsequent research, we plan to evaluate the effectiveness of the EDC method introduced in [14] for determining the equivalent dielectric constant of the dielectric tube. Additionally, we examine the current distribution across the surface of tapes with varying widths, especially in the context of rectangular helix TWTs. With the advent of micro machining printed fabrication techniques, rectangular SWS with inclined straight edge connections, as mentioned in this manuscript, and further smaller dimensions can be fabricated, thereby leading to high-frequency, low-power signal amplifications.

REFERENCES

[1] Kalyanasundaram, N. and G. N. Babu, "Dispersion of electromagnetic waves guided by an open tape helix I," *Progress In Electromagnetics Research B*, Vol. 16, 311–331, 2009.

[2] Joshi, S. N. and B. N. Basu, "Equivalent circuit analysis of a practical slow-wave structure for TWT's," *IETE Journal of Research*, Vol. 25, No. 10, 423–425, 1979.

[3] Kalyanasundaram, N. and G. N. Babu, "Propagation of electromagnetic waves guided by the anisotropically conducting model of a tape helix supported by dielectric rods," *Progress In Electromagnetics Research B*, Vol. 51, 81–99, 2013.

[4] Ghosh, S., P. K. Jain, and B. N. Basu, "Rigorous tape analysis of inhomogeneously-loaded helical slow-wave structures," *IEEE Transactions on Electron Devices*, Vol. 44, No. 7, 1158–1168, Jul. 1997.

[5] Jain, P. K. and B. N. Basu, "The inhomogeneous dielectric loading effects of practical helix supports on the interaction impedance of the slow-wave structure of a TWT," *IEEE Transactions on Electron Devices*, Vol. 39, No. 3, 727–733, Mar. 1992.

[6] Babu, G. N. and R. J. Stanislaus, "Propagation of electromagnetic waves guided by perfectly conducting model of a tape helix supported by dielectric rods," *IET Microwaves, Antennas & Propagation*, Vol. 10, No. 6, 676–685, Apr. 2016.

[7] Kalyanasundaram, N., G. N. Babu, and R. Tulsian, "On the distribution of current on an open tape helix," *Progress In Electromagnetics Research M*, Vol. 12, 81–93, 2010.

[8] Kalyanasundaram, N. and G. N. Babu, "Perfectly conducting tape-helix model for guided electromagnetic wave propagation," *IET Microwaves, Antennas & Propagation*, Vol. 6, No. 8, 899–

907, Jun. 2012.

[9] Babu, G. N., "Comparative study of guided electromagnetic wave propagation for two models of an open tape helix," *IEEE Transactions on Antennas and Propagation*, Vol. 71, No. 4, 3450–3459, Apr. 2023.

[10] Stanislaus, R. J. and N. B. Gnanamoorthi, "Large-signal field analysis of a linear beam travelling wave tube amplifier for the anisotropically conducting tape helix slow-wave structure supported by dielectric rods," *Journal of Electromagnetic Waves and Applications*, Vol. 32, No. 4, 439–470, 2018.

[11] Arora, R. K., "Surface waves on a pair of parallel undirectionally conducting screens," *IEEE Transactions on Antennas and Propagation*, Vol. 14, No. 6, 795–797, 1966.

[12] Chadha, D., S. Aditya, and R. Arora, "Field-theory of planar helix traveling-wave tube," *IEEE Transactions on Microwave Theory and Techniques*, Vol. 31, No. 1, 73–76, 1983.

[13] Aditya, S. and R. Arora, "Guided-waves on a planar helix," *IEEE Transactions on Microwave Theory and Techniques*, Vol. 27, No. 10, 860–863, 1979.

[14] Kumar, A. M. M. and S. Aditya, "Simplified tape-helix analysis of the planar helix slow wave structure with straight-edge connections," *IEEE Transactions on Electron Devices*, Vol. 65, No. 6, 2280–2286, Jun. 2018.

[15] Fu, C., Y. Wei, W. Wang, and Y. Gong, "Dispersion characteristics of a rectangular helix slow-wave structure," *IEEE Transactions on Electron Devices*, Vol. 55, No. 12, 3582–3589, Dec. 2008.

[16] Fu, C.-F., Y.-Y. Wei, W.-X. Wang, and Y.-B. Gong, "Radiofrequency characteristics of a printed rectangular helix slow-wave structure," *Chinese Physics Letters*, Vol. 25, No. 9, 3478–3481, Sep. 2008.

[17] Wei, W., Y. Wei, W. Wang, M. Zhang, H. Gong, and Y. Gong, "Dispersion equations of a rectangular tape helix slow-wave structure," *IEEE Transactions on Microwave Theory and Techniques*, Vol. 63, No. 5, 1445–1456, May 2015.

[18] Meixner, J., "The behavior of electromagnetic fields at edges," *IEEE Transactions on Antennas and Propagation*, Vol. 20, No. 4, 442–446, 1972.

[19] Marcatili, E. A. J., "Dielectric rectangular waveguide and directional coupler for integrated optics," *Bell System Technical Journal*, Vol. 48, No. 7, 2071–2102, 1969.

[20] Kumar, A. M. M., S. Aditya, and C. Chua, "Interaction impedance for space harmonics of circular helix using simulations," *IEEE Transactions on Electron Devices*, Vol. 64, No. 4, 1868–1872, Apr. 2017.